Advances in Science and Technology Research Journal

Advances in Science and Technology Research Journal 2024, 18(2), 374–384
https://doi.org/10.12913/22998624/185409
ISSN 2299-8624, License CC-BY 4.0

Received: 2023.12.19
Accepted: 2024.02.23
Published: 2024.03.15

Modification of Microstructure and Surface Properties of Ti-6Al-4V Alloy by Molybdenum Disilicide Particles Using Micro-Arc Oxidation Process

Nawar Fahem Kadhim[1*], Ali Hubi Haleem[1], Samir Hamid Awad[1]

[1] College of Materials Engineering, University of Babylon, Iraq

* Corresponding author's e-mail: aboamna299@gmail.com

ABSTRACT

As an effective surface modification technique, micro-arc oxidation (MAO) is now widely used to improve the hardness and wear resistance of Ti and its alloys by low-cost and thick ceramic coatings. In this study, molybdenum disilicide ($MoSi_2$) – modified ceramic coatings were deposited on Ti–6Al–4V alloy (340 HV) by MAO using an aqueous solution of Na_2SiO_3, $(NaPO_3)_6$ and NaOH and $MoSi_2$ particles. $MoSi_2$ particles (3, 5, and 7 g/l) from wastes of furnaces electrodes were introduced into the electrolyte to improve the microstructure and surface properties of Ti-6Al-4V alloys. A scanning electron microscope (SEM), dispersive spectroscopy (EDS), X-ray diffraction (XRD), and mechanical tests (microhardness and wear) were used to identify the coating properties, morphologies, and phases. The findings showed that the addition of 5 g/l $MoSi_2$ increased the thickness and hardness of MAO coatings from 19.08 µm and 910 HV to 33.12 µm and 1260 HV, respectively. Also, the wear resistance by means of weight losses of uncoated alloys enhanced by 68% and 100% after MAO and 5 g/l $MoSi_2$ modified-MAO coatings, respectively. Results of this work will promote future works in using of industrial wastes in surface engineering of Ti-6Al-4V alloys by MAO technique for wear resistance applications.

Keywords: Ti6Al4V, micro arc oxidation, hardness, wear, molybdenum disilicide.

INTRODUCTION

Titanium and its alloys such as Ti-6Al-4V as lightweight metals of high relative mechanical strength and fatigue limit, unique properties, including superior biocompatibility, superconductivity, and shape memory, are widely employed in the aerospace, medical equipment, and chemical industries, marine applications at moderate costs, and are found in different branches of modern industry [1-5]. However, these alloys can't be used into mechanical parts that are prone to friction, due to their tribological nature. In actuality, friction between a titanium part and another mechanical part, regardless of the materials in contact, especially for a titanium/titanium contact, intensifies the seizure phenomenon. There are numerous techniques that are frequently used to enhance the surface properties of titanium alloys for wear resistance applications [6], heavy friction condition, including plasma spraying [7], physical vapor deposition (PVD), and chemical vapor deposition (CVD) [8], but their preparation processes are complex, their costs are comparatively high, and their bonding forces are weak. Micro-arc oxidation (MAO) is a revolutionary surface treatment method that is easy to use, effective, and safe for the environment. Excellent surface properties can be obtained by micro-arc oxidizing alloys with the right process parameters [9-11]. Among reported coatings, $MoSi_2$-based coatings are demonstrated to exhibit it improve surface for heavy engineering applications like military equipment, industrial-technological systems, automotive parts, farming fitting, sporting goods, and biomedical engineering [13, 14], by increasing not just the service life of essential components but also the alloys ability to tolerate harsher

service environments [15]. As is well known, the electrolytes composition has a significant impact on the MAO coatings performance [16, 17]. Phosphate [18], and silicate-based electrolytes are currently the most widely used electrolyte systems. The performance of the MAO coatings can be improved by using mixed electrolytes (such as phosphoric acid-silicic acid electrolyte), notwithstanding the drawbacks of single electrolyte systems. Recent studies have attempted to improve the surface properties of the coating by adding tungsten trioxide (WO_3), magnesium oxide (MgO), cerium oxide (CeO_2), and sodium stannate (Na_2SnO_3) to the MAO electrolyte [19]. Their research demonstrated that these additives can improve coatings corrosion resistance and wear resistance. Recently, the use of Industrial wastes in surface engineering and composite materials is becoming increasingly required to reduce pollution and production costs, and will contribute to wastes disposal and green engineering [20, 21].

In this work, $MoSi_2$ particles from wastes of furnaces electrodes were used to modify the MAO coatings on Ti6Al4V alloys. Their effects on hardness and wear resistance were investigated.

EXPERIMENTAL WORK

Materials

Ø 30 rod of Ti6Al4V (Grade 5) alloy was used for preparation of Ø 16×5 mm disc substrates using wire EDM cutting, Its chemical make-up is displayed in Table 1. The substrates were cleaned with ultrasonic agitation in acetone, rinsed with deionized water, and dried in warm air before being successively ground and polished with SiC abrasive sheets ranging from 180 to 3000 grit.

Wastes from furnaces heating elements were used to prepare $MoSi_2$ particles. Manually kibbling of the elements was performed to get the quasi finished powders. Then, the powder was milled for 10 hours using a ball mill at speed 200 rpm. After that, the particle size distribution of the powder was determined using a (Better size 2000 particle size analyzer), it was with mean diameter of Ø 3.2 μm. The oxides contents and other components in the powder were determined using X-ray fluorescence (XRF) as shown in Table 2.

MAO process

A 500V DC-AC homemade MAO deposition unit shown in Figure 1 was used to deposit the ceramic coatings at current density 3 mA/cm^2 and voltage of 320 V for 50 minutes. In the plastic container, one liters of electrolyte was agitated and cooled using a mechanical Stirrer and cooling system to prevent electrolyte solution heating over to 20 °C. Composition of MAO electrolyte is shown in Table 3. The electrolyte solutions were mixed for 15 min. before MAO process. All sample were rinsed in distilled water, and dried in air after coating.

Characterizations

An X-ray diffractometer system (XRD-Aeris Panalaytival Company / Dutch Origin) was used to identify the coatings, where the scan rate was 0.02, and the scanning step was 0.5 degree/min. The microstructure and surface morphology ,and coating thickness was studied using scanning electron microscope SEM (Axia Chemi Sem Thermo Scintific Company/Dutch Origin) with energy dispersive spectros copy EDS for the analysis of chemical composition of coatings. Atomic force microscopy AFM, model (Core AFM Nanosurf-Switzerland) was used to observe topography and roughness of coatings by means of arithmetic mean height (Sa). With a force of 10 N and a holding period of 15 seconds, the Vickers indenter (HVS-1000, Larsee, Digital Microhardness Tester) was used to measure the microhardness to ASTM E3841,

Table 1. Chemical composition of Ti6Al4V (Grade 5) (according to the manufacturers` certificates)

Element	Al	V	Fe	C	N	H	O	Ti
Weight%	4.5-5.9	3.9 - 4	≤ 0.30	≤ 0.1	≤ 0.05	≤ 0.015	≤ 0.20	Bal.

Table 2. Chemical composition of $MoSi_2$ powder

Element	Ni	Co	Fe	C	Nb	Cu	W	Mo
Weight%	0.052	0.0625	0.237	≤ 0.1	0.270	0.285	≥ 14.39	Bal.

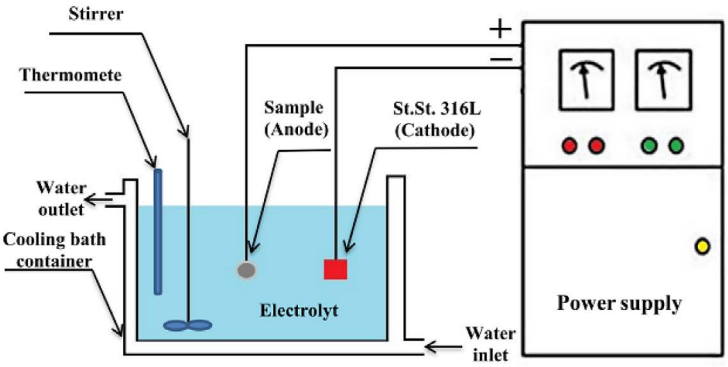

Fig. 1. The coating unit of MAO

Table 3. Composition of MAO electrolyte

Sample No.	Components (g/l)			
	$NaSiO_2$	$(NaPO_3)_6$	NaOH	$MoSi_2$
A	10	8	2	-
B	10	8	2	3
C	10	8	2	5
D	10	8	2	7

the average of 3 measurements was considered as an average value of HV to minimize the standard deviation SD [22].

A ball-on-disk tribometer (TBR Anton Paar) shown in Figure 2 was used to evaluate the friction and wear resistance behavior of coated and uncoated substrate using zirconia pin at room temperature. The circular module was used to operate the tribometer, and the parameters for circular friction are listed in Table 4. The wear resistance was determined by means of weight losses because it gives a clear indication of wear [7, 23]. The sensitive balance type (L2205-D, Germany) was used for measurement of the reliable weight losses.

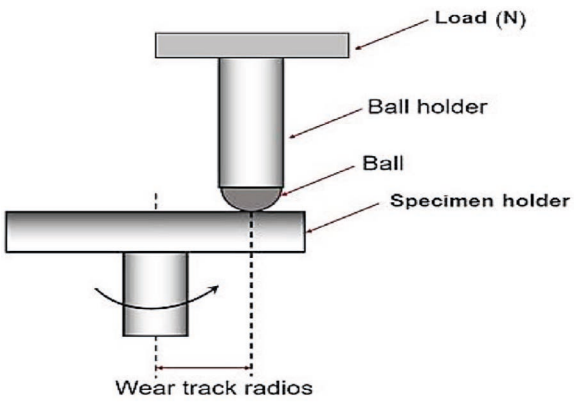

Fig. 2. Schematic diagram for ball-on-disk testing [24]

Table 4. Ball-on-disk testing parameters

Friction module	Circular friction
Load	6 N
Ball diameter	6 mm
Frequency/ Rotating speed	477 rpm
Cycle number	5
Dry conditions	yes
Sliding distance	0.15 m/s

RESULTS AND DISCUSSION

Initially, it is of great importance to declare that, compared to the results of sample C, samples B and D could not show the promised results in terms of microhardness and wear resistance, which are among the objectives of the research. Therefore, the results of sample C were relied upon and compared to the base sample for the purpose of evaluating the research objectives.

SEM observation, EDS and XRD analysis

Figures 3 and 4 show fracture cross-section micrographs of MAO coating (sample A and C) and (sample B and D), respectively. It can be observed that the coatings are thick [25, 26], and the outer layer is porous for A,B and D samples, however, the inner layer is relatively dense [27], with

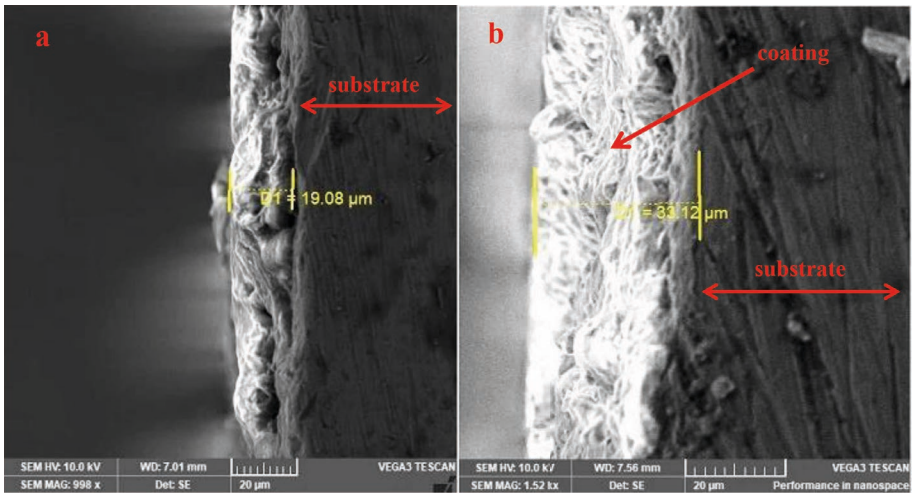

Fig. 3. SEM micrographs of MAO coating of samples: (a) A, (b) C

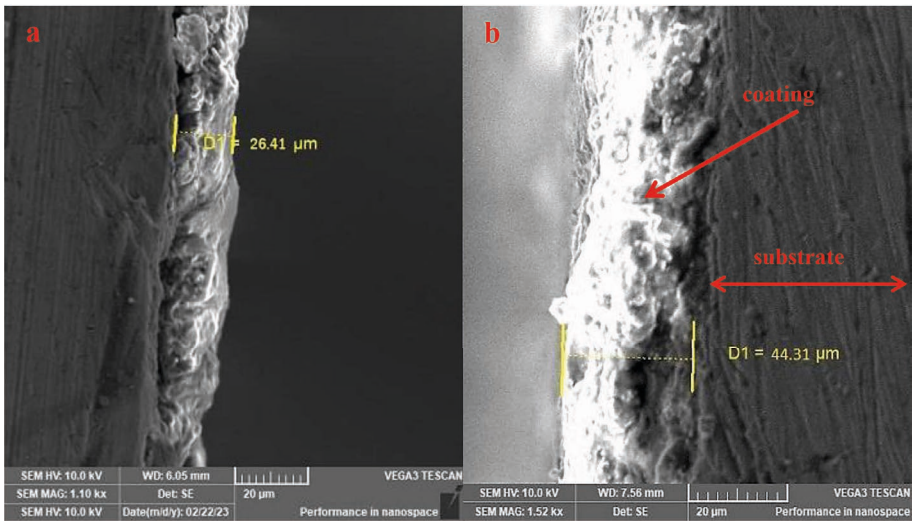

Fig. 4. SEM micrographs of MAO coating of samples: (a) B, (b) D

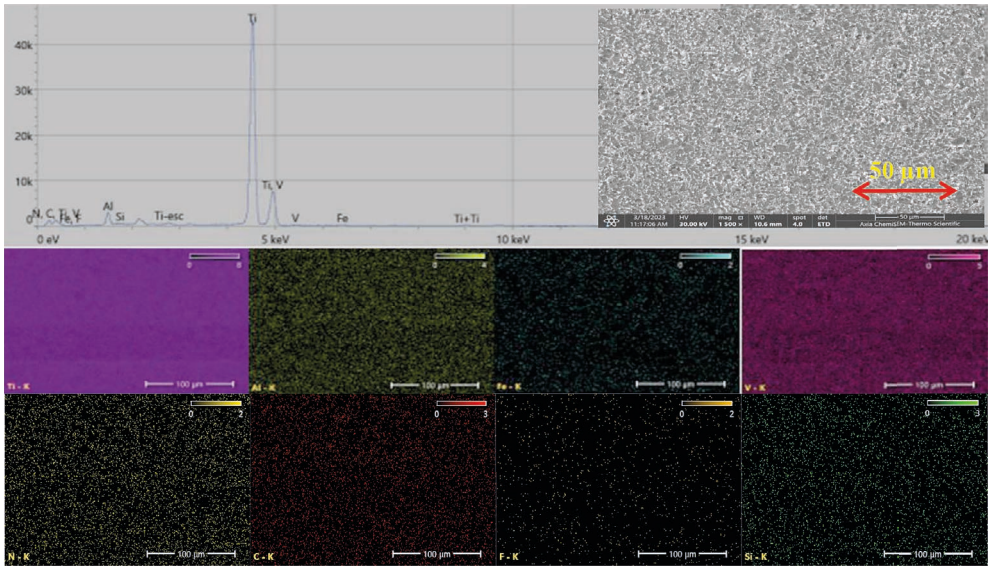

Fig. 5. SEM micrographs and EDS results of uncoated substrates

a good adhesion to the substrate. Also, it can be observed, the regulation of coating density sample C, furthermore, the coating layer is uniform and has a relatively uniform thickness along the sample surface, the interface between the coating and the substrate is also regular and homogeneous almost along the sample surface.

Uncoated and coated substrates surface morphologies and their EDS spectra are shown in Figures (5, 6, and 7) with different magnifications.

The EDS results of uncoated substrate (Fig. 5) indicate the clear presence of elements from the Ti6AI4V composition such as Al ,V, and C also, the existence of oxygen element can be attributed to natural thin TiO_2 formation on the surface by oxidation [28]. The EDS results of the coated substrates (Figures 6, and 7) show a considerable increase in oxygen content, suggestive the coating should be a combination of titanium oxides and modification elements from the electrolyte such Si, V,O and Ti alloy composition. Most likely, the metallurgical intermixing and interdiffusional bonding generated real by the micro-arcing process creates a high degree of interfacial adhesion

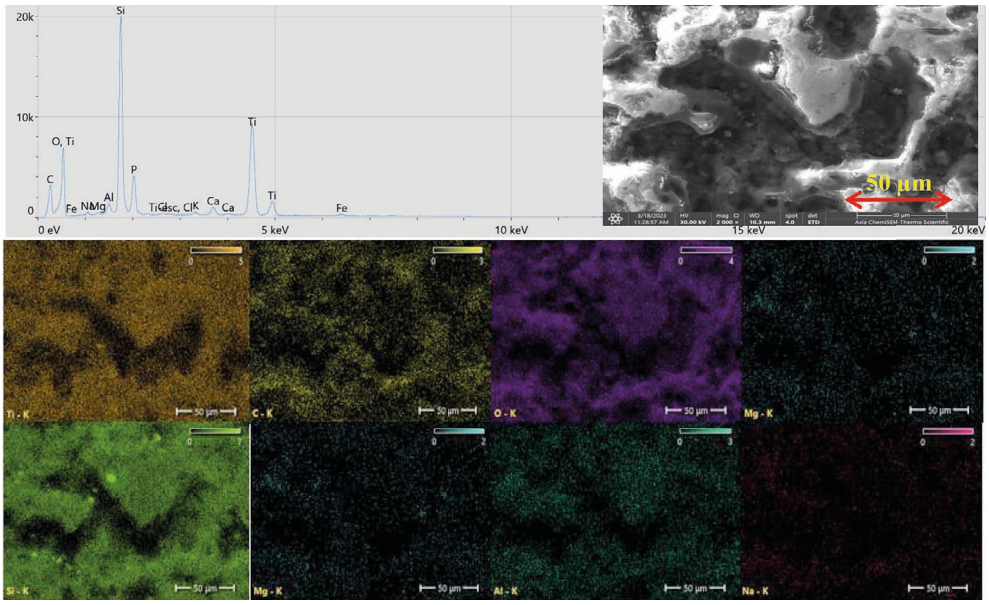

Fig. 6. SEM micrographs and EDS results of sample A

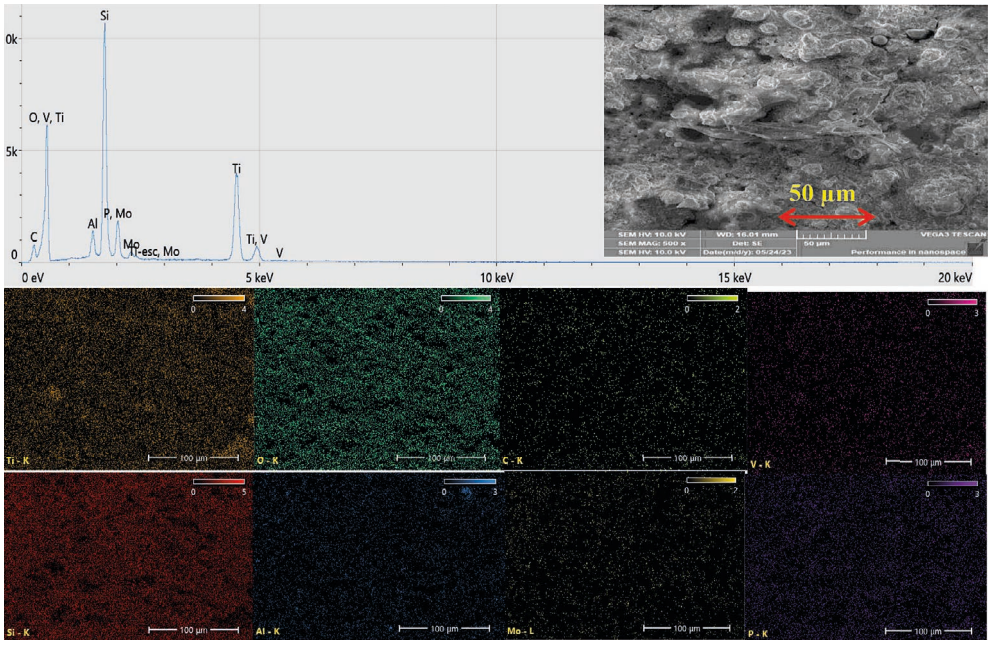

Fig. 7. SEM micrographs and EDS results of sample C

between coating and substrate. It can observed the appearance of (Si) content in the sample A, which comes from the electrolyte. The increase in the appearance of (Si) content in the sample (C) came from addition of $MoSi_2$ and the appearance of Mo content was also observed. This can prove the success of current work in depositing MAO layer modified with $MoSi_2$.

XRD spectra of MAO coating modified by $MoSi_2$ addition is shown in Figure 8. It can be concluded that the modified coatings had a structure and composition consisting of a mixture of Antase Ti, Rutile Ti, and $MoSi_2$. Also, they prove the deposition of $MoSi_2$ modified titanium oxides. The deposition of titanium oxide on substrate surfaces was demonstrated by XRD patterns. The standard cards (JCPDS No.010-0425) indicated that the mean peaks were TiO_2 (antase and rutile). TiO_2 dominant peaks were found at 2θ values of 37.77°, 44.70°, and 79.10°.The $MoSi_2$ peaks were identified in accordance with the JCPDS No. 004-0787 standard cards. The positions of these peaks at 2 θ were 41.29°, 44.67°, and 77.60°. The $MoSi_2$ peaks observed are attributed to incorporation of MoSi2 particles in the coating which resulted in thick MAO coating. There were not many deviations between the $MoSi_2$ diffraction at various 2θ obtained in this work and those from standard specifications. This discrepancy is most likely due to variations in the $MoSi_2$ preparation procedures as well as the precision and conditions of acquiring the diffraction data [29]. Most likely, the big background of amorphous phases observed in the XRD patterns indicated for the deposition of the glassy phases which always leach on the surface of $MoSi_2$ particles due to the heating of furnaces electrodes during the service. Moreover such glassy phases had their significant effects in immersing the pores in the coating and give it a glassy nature or glassy behaviour.

AFM analysis

Figure 9 and Table 5 show the results of AfM test. The AfM images reveal the form and particle size distribution of the coated layers, which represented the asperities and cusps of the surface. It can be observed from the figures, that the coating were dense with cusps had different mean diameters and distribution in the surface topography. Such cusps and their characterization by Sa 57.60 nm and density 16527052 particles/mm² are given in Table 5.

In general, results of densities from table are in agreement with observed at the in agreement with those observed at the figures. MAO coating modified by $MoSi_2$ particles (sample C) recorded the highest density among the others. Also, after MAO coating the surfaces characterized with higher roughnesses and densities in comparison to those uncoated substrates.

Table 5. AFM roughness for uncoated, A and C samples modification of MAO coating with $MoSi_2$ particles resulted in roughness decreased from 73.30 nm to 57.60 nm

Sample No.	Roughness nm (Sa)
Uncoated	18.73
A	73.30
C	57.60

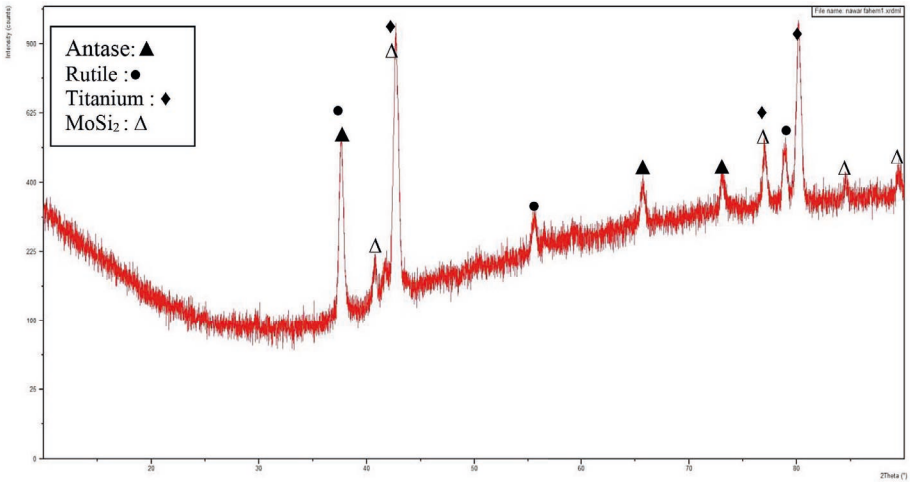

Fig. 8. XRD pattern of $MoSi_2$ – modifed TiO_2 coatings (sample C)

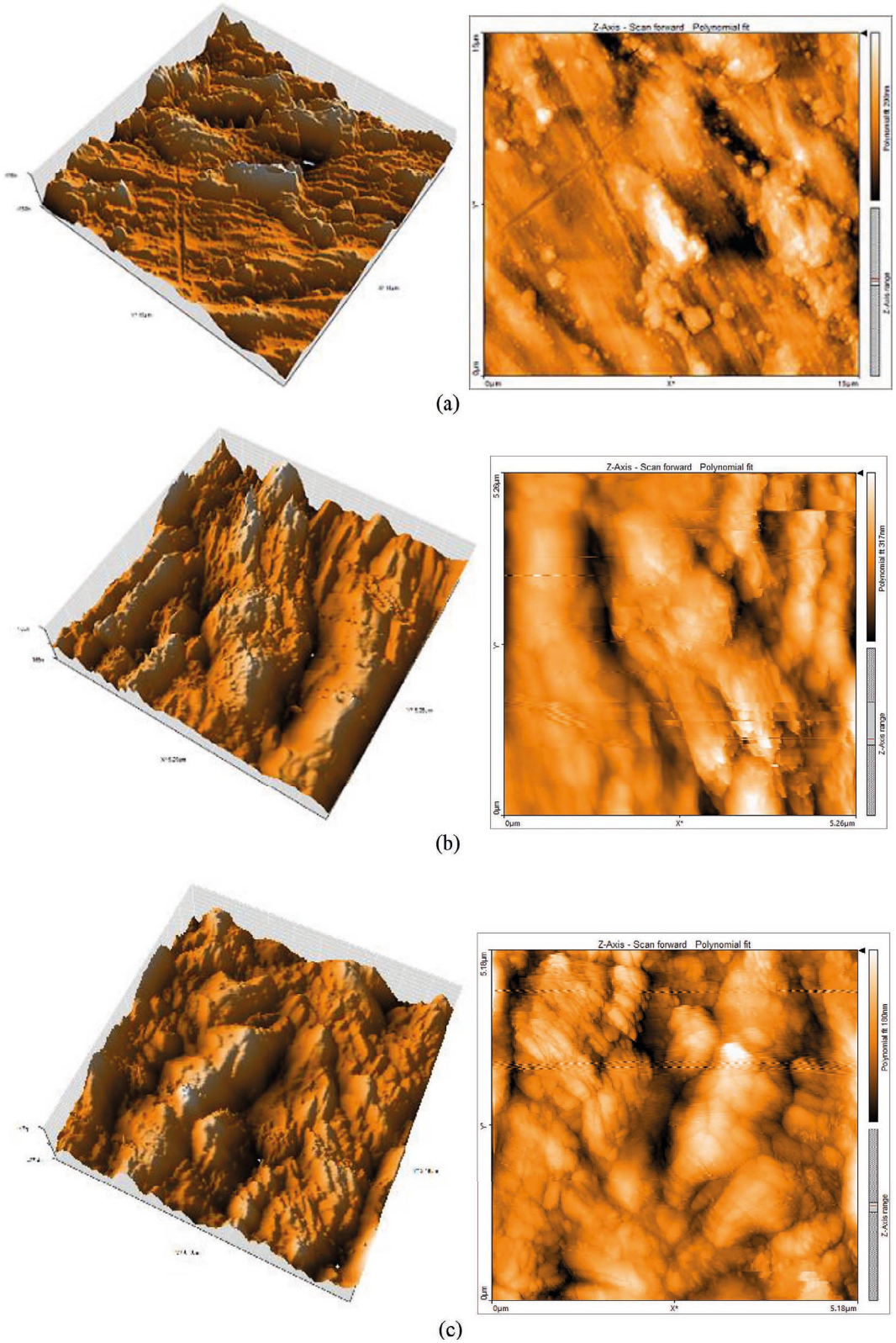

Fig. 9. AFM results of: (a) uncoated, (b) A, (c) C, samples

Coating thickness and hardness

The results indicated that as the thickness of the outer layer and close of porosity, the hardness values increased with adding of $MoSi_2$, which significantly improved the micro hardness value Most likely, the hardness and wear resistance properties important factors such as coating structure and of coatings are more strongly affected by morphologies, and pores distribution

than coatings thickness[30]. Furthermore, different sizes of pan-like or sphere-like geometric pores, which are the result of the molten liquid that swiftly hardened and left distinct borders around the pores, characterize the morphologies that may be observed in the structure. The quick solidification observed in sample (A) (Fig. 6). due to the constant exposure of molten oxide to cold electrolyte caused the formation of microcracks on the morphology. While in sample C (Fig. 7), because of the extremely high temperatures at the sparking spots sites, the metal from the substrate and its oxide melt and shoot out of the discharge tunnels. As seen in Figure 7 (sample C), it is evident that this melted oxide, represented by the white particles in the SEM data, increases with the addition of $MoSi_2$. This, in turn, increased the micorhardness while decreasing porosity and uneven distribution. Sample structure was generally characterized by a non-uniform distribution of pores. Taking into account the uneven distribution of porosity, sample hardness was 910 HV may be impacted [31], in comparison with sample (C). As expected, adding of $MoSi_2$ contributed to giving hardness of 1260 HV [32]. Table 6 shows the results of thickness and microhardness. It can be observed that the MAO coatings with thickness of 19.08–44.31 μm increased the hardness of the substrate, from 340 HV to hardness values in the range 645–1260 HV. In general, such improvement in hardness values can be attributed to the formation of surface oxides by the MAO process which were mainly composed of anatase and rutile modifications of TiO_2 (Fig. 7) [33, 34]. It should be noted that, the surface pores number, anatase /rutile phase ratio, and coating thickness can influence the hardness values [35].

Also, with the increasing of $MoSi_2$ addition from 3 g/l to 5 g/l (sample C), the hardness and thickness of MAO coatings increased from 910 HV, and 19.02 μm to 1260 HV, and 33.42 μm, respectively. The significant increase in hardness can be attributed to the addition of modification elements such as Mo and W (refractory elements) characterized by their high hardness and resistance to heat. In addition, on the relevant XRD patterns of sample C (Fig. 7) anatase peaks were weaker when compared to those of rutile, because anatase-dominated oxide layers generally form at voltages as low as 250 V [33]. The rutile phases are more effective than those anatase phases in formation of hard surfaces. However, MAO coatings after the addition of 7 g/l $MoSi_2$ gave a lower hardness (645 HV) compared to other $MoSi_2$ modified coatings (3 and 5 g/l) due the effects of pores distribution and morphology on their thickest (44.31 μm) coatings.

Table 6. Results of thicknesses and microhardness

Simple No.	Thickness (μm)	Microhardness (HV)
Uncoated substrate	-	340 ± 5
A	19.08	910 ± 3
B	26.41	930 ± 7
C	33.12	1260 ± 7
D	44.31	645 ± 10

Dry sliding tests

Results from wear test carried out for different times (30, 60, 90, 120 and 150 min) are shown in Figure 10. The results proved the significant effects of MAO coatings after the addition of $MoSi_2$ particles in sample (C) in decreasing the weight losses in comparison to the uncoated sample, coated sample (A) and with addition of $MoSi_2$ particles for (B and D) samples, as shown in Figure 10. In general, the weight losses varied with duration of rubbing and normal load at constant sliding velocity, and there were some „negative weight losses" for coating C. The explanation for this case is that the surface of the sample contained asperities, and at the beginning of the test the frictional thrust increased, which resulted in increased debonding and sub-surface fracture of the asperities, and thereafter ,led to a clear loss of weight for ascertain duration of rubbing. After that, the surface was becoming smoother and the loss of weight remained almost non-existent, for

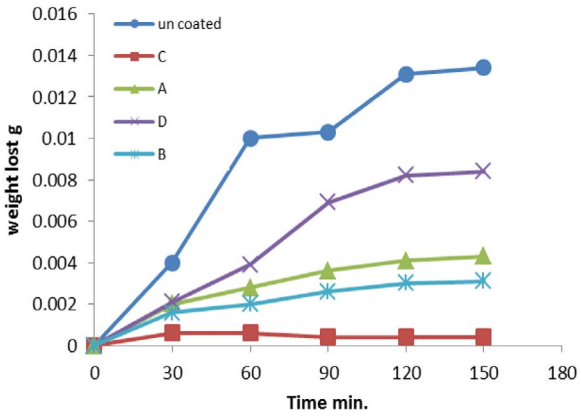

Fig. 10. Results of wear test

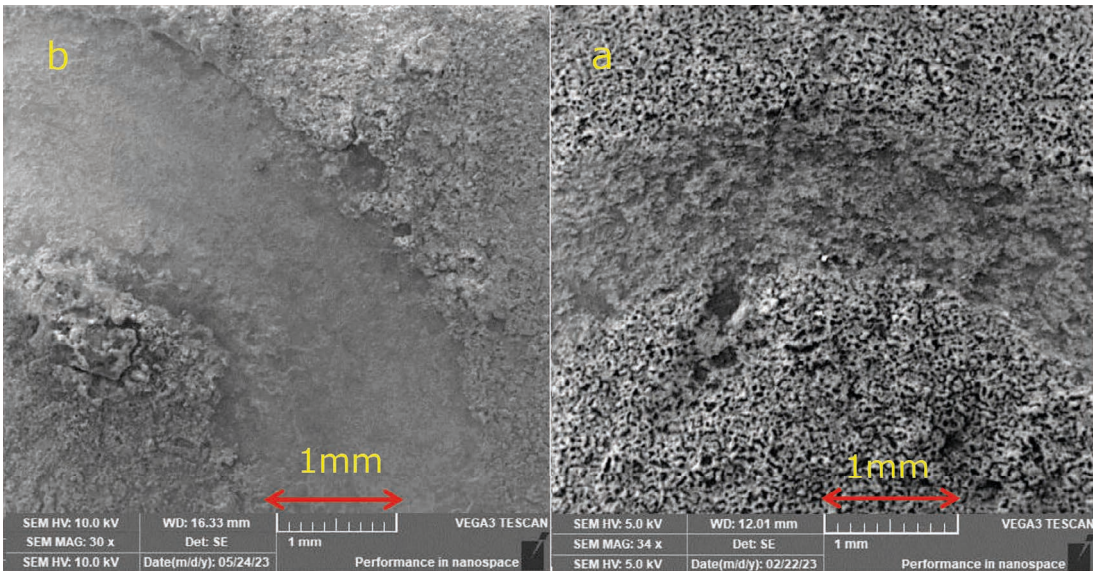

Fig. 11. SEM images of worn surfaces for: (a) MAO coating (sample A), (b) $MoSi_2$ – modified MAO coating (sample C)

the rest of the experimental time due to the nature of the improved properties of coatings surfaces, which could give high resistance to wear.

Furthermore, the incorporation of $MoSi_2$ recorded the best improving in wear resistance among the other samples due to the high mechanical properties of $MoSi_2$ particles and their effects in filling the micropores [36], and therefore reducing the surface roughens. Hardness is not the only thing that plays a significant role in wear, but there are other factors such as the uniformity of the surface as well as the adhesion of the coated to the substrate and the absence of voids between them, and this is shown by the cross-sectional images of the SEM in the Fig. 3). The wear resistance of samples B and D low in comparison to that of sample C.

The MAO coating in sample A contained a large number of micropores and microcracks, as seen in Figure 10a. When the coating was applied to zirgonia balls, the micropores caused an uneven friction force and a higher surface roughness Sa = 73.30 µm. Poor tribological characteristics came from some micro-cracks that were easily ground off the surface and generated debris as the friction increased [37]. This plowed the coated surface, as a result, a significant quantity of debris was seen on the MAO coating deteriorated surface. On the other hand, $MoSi_2$ microparticles were present in the micropores of the $MoSi_2$-modified MAO coatin, and so reduced the surface roughness Sa = 57.60 µm, as shown in Figure 10b for the sample C [38].

CONCLUSIONS

Based of results obtained the following conclusions can be drown:

1. On Ti6Al4V alloy substrates, hard and thick $MoSi_2$-containing TiO_2 ceramic coatings can be deposited using MAO electrolytes modified by $MoSi_2$ additions from industrial wastes.
2. Characterization of the modified coatings by the XRD, SEM and EDS proved the deposition of rutile and anatase phases in TiO_2 coatings with microstructures characterized with varying pore sizes and distributions.
3. The addition of $MoSi_2$ enhanced the hardness, reduced the pores in coatings, resulted in thick, compact, and dense coatings, therefore increased the wear resistance by means of weight losses.
4. Unmodified MAO coatings with thickness of 19.08 µm increased the hardness of Ti6Al4V alloy substrates from 340 HV to 910 HV, while the addition of 3 g/l and 5 g/l $MoSi_2$ increased the thickness and hardness of the MAO coatings to 26.4 µm and 930 HV, and 33.12 µm and 1260 HV, respectively.
5. The addition of 3 g/l and 5 g/l $MoSi_2$ showed great improvements 51%, and 100%, respectively in the wear resistance of the Ti6Al4V alloy substrates .
6. The non-uniform distribution of pores and their densities in the significantly affected the hardness differences, and wear resistance property.

REFERENCES

1. Xin G., Wu C., Cao H., Liu W., Li B., Huang Y., Rong Y., Zhang G. Super hydrophobic TC4 alloy surface fabricated by laser micro-scanning to reduce adhesion and drag resistance. Surface and Coatings Technology, 2020, 391, 125707.
2. Zhang S., Zhao C., Zhang J., Lian Y., He Y. C-Al_2O_3 coatings prepared by cathode plasma electrolytic deposition on TC_4 substrate for better high temperature oxidation resistance. Surface and Coatings Technology, 2021, 405, 126585.
3. Xie R., Lin N., Zhou P., Zou J., Han P., Wang Z., Tang B. A surface damage mitigation of TC4 alloy via micro arc oxidation for oil and gas exploitation application: Characterizations of microstructure and evaluations on surface performance. Applied Surface Science, 2018, 436, 467-476.
4. Jażdżewska M., Majkowska-Marzec B., Ostrowski R., Olive J.-M. Influence of surface laser treatment on mechanical properties and residual stresses of titanium and its alloys. Advances in Science and Technology Research Journal 2023, 17(6), 27–38.
5. Majkowska-Marzec B., Sypniewska J. Microstructure and mechanical properties of laser surface-treated ti13nb13zr alloy with mwcnts coatings. Advances in Materials Science, 21(4) 70, 2021.
6. Yamanoglu R., Fazakas E., Ahnia F., Alontseva D., Khoshnaw F. Pitting corrosion behaviour of austenitic stainless-steel coated on Ti6Al4V alloy in chloride solutions. Advances in Materials Science, 2021, 21, 2(68).
7. Lai-Chang Zhang, Liang-Yu Chen, Liqiang Wang. Surface modification of titanium and titanium alloys: technologies, developments and future interests. Advanced Engineering Materials, 2020, 22(5), 1901258.
8. Quanzhi Chen, Zhiqiu Jiang, Shiguang Tang, Wanbing Dong, Qing Tong, Weizhou Li. Influence of graphene particles on the micro-arc oxidation behaviors of 6063 aluminum alloy and the coating properties. Applied Surface Science, 2017, 423, 939-950.
9. Wei Yang, Shangkun Wu, Dapeng Xu, Wei Gao, Yuhong Yao, Qiaoqin Guo, Jian Chen. Preparation and performance of alumina ceramic coating doped with aluminum nitride by micro arc oxidation. Ceramics International, 2020, 46(10) Part B, 17112-17116.
10. Dzhurinskiy D., Gao Y., Yeung W.-K., Strumban E., Leshchinsky V., Chu P.-J., Matthews A., Yerokhin A., Maev R.Gr.. Characterization and corrosion evaluation of TiO_2:n-HA coatings on titanium alloy formed by plasma electrolytic oxidation. Surface and Coatings Technology, 2015, 269, 258-265.
11. Wheeler J.M., Collier C.A., Paillard J.M., Curran J.A. Evaluation of micromechanical behaviour of plasma electrolytic oxidation (PEO) coatings on Ti–6Al–4V. Surface and Coatings Technology, 2010, 204(21–22), 3399-3409.
12. Jingtao Wang, Yaokun Pan, Rui Feng, Hongwei Cui, Benkui Gong, Lei Zhang, Zengli Gao, Xiaoli Cui., Hongbin Zhang, Zhiqiang Jia. Effect of electrolyte composition on the microstructure and biocorrosion behavior of micro-arc oxidized coatings on biomedical Ti6Al4V alloy. Journal of Materials Research and Technology, 2020, 9(2), 1477-1490.
13. Saurabh A., Meghana C.M., Singh P.K., Verma P.C. Titanium-based materials: synthesis, properties, and applications. Materials Today: Proceedings, 2022, 56, 412–419.
14. Pesode P., Barve S., Wankhede S.V., Jadhav D.R., Pawar S.K. Titanium alloy selection for biomedical application using weighted sum model methodology. Materials Today: Proceedings, 2023, 72, 724–728.
15. Carabat A.L., Meijerink M.J., Brouwer J.C., Kelder E.M., van Ommen J.R., van der Zwaag S., Sloof W.G. Protecting the $MoSi_2$ healing particles for thermal barrier coatings using a sol-gel produced Al_2O_3 coating. Journal of the European Ceramic Society, 2018, 38(7), 2728-2734.
16. Zhongren Zheng, Ming-Chun Zhao, Lili Tan, Ying-Chao Zhao, Bin Xie, Dengfeng Yin, Ke Yang, Atrens A. Corrosion behavior of a self-sealing coating containing CeO_2 particles on pure Mg produced by micro-arc oxidation. Surface and Coatings Technology, 2020, 386, 125456.
17. Wei Yang, Dapeng Xu, Xiaofei Yao, Jianli Wang, Jian Chen. Stable preparation and characterization of yellow micro arc oxidation coating on magnesium alloy. Journal of Alloys and Compounds, 2018, 745, 609-616.
18. Bih-Show Lou., Jyh-Wei Lee., Chuan-Ming Tseng., Yi-Yuan Lin., Chien-An Yen. Mechanical property and corrosion resistance evaluation of AZ31 magnesium alloys by plasma electrolytic oxidation treatment: Effect of MoS_2 particle addition. Surface and Coatings Technology, 2018, 350, 813-822.
19. Chen X.W., Li. M.L, Zhang D.F., Cai L.P., Ren R., Hu J., Liao D.D. Corrosion resistance of MoS_2-modified titanium alloy micro-arc oxidation coating. Surface and Coatings Technology, 2022, 433, 128127.
20. Erdoğan A., Gök M.S., Koç. V., Günen A. Friction and wear behavior of epoxy composite filled with industrial wastes. Journal of Cleaner Production, 2019, 237, 117588. doi: 10.1016/j.jclepro.2019.07.063.
21. Aigbodion V.S., Akinlabi E.T. Explicit microstructural evolution and electrochemical performance of zinc-eggshell particles composite coating on mild steel. Surfaces and Interfaces, 17, 2019, 100387.
22. Berthod P. Room temperature hardness of carbides-strengthened cast alloys in relation with their carbon content and the aging temperature, Part I: Case of

nickel alloys. Materials Science and Technology, 2009, 25(5), 663-669.

23. Zhecheva A., Sha W., Malinov S., Long A. Enhancing the microstructure and properties of titanium alloys through nitriding and other surface engineering methods. Surface & Coatings Technology, 2005, 200(7), 2192–2207.
24. Nan Ye, Yunzhu Ma, Jiancheng Tang. Microstructure and wear resistance of bimodal cemented carbide coating prepared by direct laser powder deposition. Materials Research Express, 221, 8, 066508.
25. Carter C.B., Norton M.G. Ceramic materials, science and engineering. Textbook. 2013, 495-508, Publisher Springer New York.
26. Belin-Ferre E. Surface properties and engineering of complex intermetallic. Book Series on Complex Metallic Alloys, 2010, 3, pp. 48.
27. Awad S.H. A new method for deposition of ceramic coating on al alloy using duplex processes of anodizing and Al_2O_3 modified electrolyte micro arc oxidation (MAO). The Iraqi Journal for Mechanical and Material Engineering, 2020, 20(4).
28. Guleryuz H., Cimenoglu H. Effect of thermal oxidation on corrosion and corrosion-wear behaviour of a Ti–6Al–4V alloy. Biomaterials, 2004, 25, 3325–3333.
29. Nie X., Leyland A., Song H.W., Yerokhin A.L., Dowey S.J., Matthews A. Thickness effects on the mechanical properties of micro-arc discharge oxide coatings on aluminium alloys. Surface and Coatings Technology, 1999, 116–119, 1055–1060.
30. Tapia-López J., Pech-Canul M.I., García H.M. Processing, microstructure, properties, and applications of $MoSi_2$-containing composites: A review. International Advanced Research Center for Powder Metallurgy and New Materials, India, 12 July 2023.
31. Khorasanian M., Dehghan A., Shariat M.H., Bahrololoom M.E., Javadpour S. Microstructure and wear resistance of oxide coatings on Ti–6Al–4V produced by plasma electrolytic oxidation in an inexpensive electrolyte. Surface & Coatings Technology, 2011, 206, 1495–1502.
32. Sameezadeh M., Emamy M., Farhangi H. Effects of particulate reinforcement and heat treatment on the hardness and wear properties of AA 2024-$MoSi_2$ nanocomposites. Materials & Design, 2011, 32(4), 2157-2164.
33. Cimenoglu H., Gunyuz M., Kose G.T., Baydogan M., Uğurlu F., Sener C. Micro-arc oxidation of Ti6Al4V and Ti6Al7Nb alloys for biomedical applications. Materials Characterization, 2011, 62, 304–311.
34. Hongbo Ba, Yuzhu Fu. Effect of micro-arc oxidation coatings with different thickness on high cycle fatigue performance of Ti-6Al-4V titanium alloy. Journal of Physics: Conference Series, 2022, 2187, 012031.
35. Cardoso G.C., Kuroda P.A.B., Grandini C.R. A detailed analysis of the MAO TiO coating hardness using the Jönsson and Hogmark "law-of-mixtures" model. Materials Letters, 2023, 352, 135208.
36. Grigoriev S., Peretyagin N., Peretyagin N., Apelfeld A., Smirnov A., Rybkina A., Kameneva E., Zheltukhin A., Gerasimov M., Volosova M., Yanushevich O., Krikheli N., Peretyagin P. Investigation of the characteristics of MAO coatings formed on Ti6Al4V titanium alloy in electrolytes with graphene oxide additives. Journal of Composites Science, 2023, 7(4), 142.
37. Wang Y.M., Lei T.Q., Guo L.X., Jiang B.L. Fretting wear behaviour of microarc oxidation coatings formed on titanium alloy against steel in unlubrication and oil lubrication. Applied Surface Science, 2006, 252, 8113–8120.
38. Lin X.Z., Zhu M.H., Zheng J.F., Luo J., Mo J.L. Fretting wear of micro-arc oxidation coating prepared on Ti6Al4V alloy. Transactions of Nonferrous Metals Society of China, 2010, 20, 537–546.